Nanoscale

RSC Publishing

PAPER

View Article Online
View Journal | View Issue

Cite this: *Nanoscale*, 2013, **5**, 6006

Understanding crystallization features of P(VDF-TrFE) copolymers under confinement to optimize ferroelectricity in nanostructures†

Mari-Cruz García-Gutiérrez,*[a] Amelia Linares,[a] Ignacio Martín-Fabiani,[a] Jaime J. Hernández,[b] Michelina Soccio,[a] Daniel R. Rueda,[a] Tiberio A. Ezquerra[a] and Michael Reynolds[c]

The successful development of ferroelectric polymer devices depends on the effective fabrication of polar ferroelectric crystalline nanostructures. We demonstrate, by scanning X-ray microdiffraction using synchrotron light, the heterogeneous character of high aspect ratio one-dimensional nanoarrays of poly(vinylidene fluoride-*co*-trifluoroethylene) copolymers supported by a residual polymer film. They were prepared by melt and solution template wetting, using porous anodic aluminum oxide as a template. The spatial evolution of different polymorphs from the mixture of paraelectric and ferroelectric crystal forms (residual film) to the pure ferroelectric form (nanoarray) is evidenced for the samples prepared by solution wetting. However, for samples prepared by melt wetting the ferroelectric phase is exclusively obtained in both the residual film and nanoarray. The crystal nuclei formed in the polymer film connected to the nanoarray play a key role in determining the formation of a crystallinity distribution gradient, where the crystallinity decreases along the first 5–10 microns in the nanorods reaching a steady value afterwards. The minimum decrease in crystallinity is revealed for samples prepared by melt wetting. The results reported in this work endeavour to enhance the understanding of crystallization under confinement for ferroelectric copolymers and reveal the parameters for improving the ferroelectric character of polymer nanostructures.

Received 29th January 2013
Accepted 24th April 2013

DOI: 10.1039/c3nr00516j

www.rsc.org/nanoscale

Introduction

Among ferroelectric materials, ferroelectric polymers have emerged as cost-effective functional materials for organic electronic devices due to their high electric breakdown field, low dielectric loss, light weight and high flexibility. Poly(vinylidene fluoride) (PVDF) and its copolymers with trifluoroethylene (TrFE) are ferroelectric polymers with a relatively high remnant polarization, large piezoelectric coefficient, high dielectric constant, and low dielectric loss.[1,2] Poly(vinylidene fluoride-*co*-trifluoroethylene) (P(VDF-TrFE)) thin films and low aspect ratio nanostructures have been extensively studied and used in various dielectric and ferroelectric device applications.[3–6] High aspect ratio (length/diameter) one-dimensional (1D) nanostructures are appropriate for studying size-dependent processes with length scales comparable to the nanostructures' size and may also have greater potential for high density energy storage applications due to the dramatically increased surface area over thin films and low aspect ratio nanostructures. There are few studies on high aspect ratio one-dimensional P(VDF-TrFE) nanostructures in the literature.[7,8] Furthermore structural heterogeneity along the 1D nanostructures is yet to be approached. While the method of nanoimprint lithography (NIL)[5,9] has been used to generate well-defined low aspect ratio nanostructures, the advantage of the template wetting technique, using porous anodic aluminum oxide (AAO) as a template, is the high versatility of the method, allowing the preparation of customized polymer nanospheres, nanotubes and nanofibers including high aspect ratio 1D nanostructures both by melt and solution wetting.[10–12]

The phase diagrams and the kinetics of phase transformation processes of matter in confined space can deviate considerably from the respective dependencies observed in bulk.[13] Polymer crystallization is an example of these phenomena as it is known that a size limitation at the nanometer scale can affect crystal nucleation, growth and orientation.[14–16] Furthermore, in a previous study concerning PVDF we have reported the crystal phase transition from the α-nonpolar crystal form with chains of an alternating *trans–gauche* conformation (TGTG) to the γ-ferroelectric crystalline structure with a

[a]*Instituto de Estructura de la Materia (IEM-CSIC), Serrano 121, 28006 Madrid, Spain. E-mail: maricruz@iem.cfmac.csic.es; Fax: +34 915645557; Tel: +34 915616800*

[b]*Institut des Sciences de Matériaux de Mulhouse, 15 rue Jean Starcky, Mulhouse, 68057, France*

[c]*ESRF, B.P. 220, F-38043 Grenoble Cedex, France*

† Electronic supplementary information (ESI) available. See DOI: 10.1039/c3nr00516j

TTTG sequence, due to PVDF confinement within nanopores and its interaction with the walls of the AAO membrane.[17] However, the most highly ferroelectric and desired crystalline form is the β-phase, where chains of all-*trans* (TTTT) conformation show iso-oriented dipoles in a pseudohexagonal crystal packing.[2] P(VDF-TrFE) copolymers crystallize more easily in the β-phase than the homopolymer PVDF because the addition of the third fluorine in the TrFE monomer unit sterically hinders the formation of the TGT conformation.[18]

The successful development of ferroelectric polymer devices depends on the effective fabrication of polar ferroelectric crystalline structures.[5,19] Indeed the aim of this study is to obtain a deeper understanding of the basis of crystallization processes under confinement and to study the heterogeneities along the 1D nanostructures in order to select the optimum parameters for improving the ferroelectric character of polymer nanoarrays.

Experimental

Sample preparation

Alumina membranes purchased from Whatman Inc. have an average pore diameter of ~25 nm (Fig. 1) which increases with pore depth reaching up to about 200 nm at the bottom of the membrane (S1). The membranes are freestanding disks of 13 mm diameter and thickness of ~60 μm. The membranes were cleaned by immersing them in hexane and applying ultrasound.

Poly(vinylidene-*co*-trifluoroethylene) P(VDF-TrFE) random copolymers with different molar concentrations ($M_n = 240\,000$ and $M_n/M_w = 1.4$),[20] supplied by Piezotech S.A.S. and Atochem (France), were infiltrated inside the AAO template by both melt and solution wetting. The infiltration into the alumina pores from the melt was carried out by placing a 200 μm thick film of the copolymer onto the AAO membrane surface at 210 °C for 30 min and then cooling down to room temperature at 20 °C min^{-1}. During the infiltration the polymer is in the molten state ($T_m \approx 160$ °C and $T_m \approx 150$ °C for the 70/30 and 80/20 compositions respectively) under nitrogen flow in order to avoid degradation. Copolymer nanostructures were also prepared by solution template wetting. A solution containing 30 wt% P(VDF-TrFE) in *N*,*N*-dimethylacetamide (Sigma-Aldrich) was prepared (the polymer/solvent concentration of 30 wt% (280 mg mL^{-1}) was chosen well above the range of concentrations reported in the literature for producing high aspect ratio polymer nanorods).[12,21] For solution wetting, the AAO membrane was placed on top of a drop of the solution and subsequently dried at 60 °C under vacuum for 20 h. Considering that the boiling point of *N*,*N*-dimethylacetamide is 165 °C, under the conditions used for the drying process, the evaporation of the solvent was slow and the subsequent crystallization conditions were well controlled.

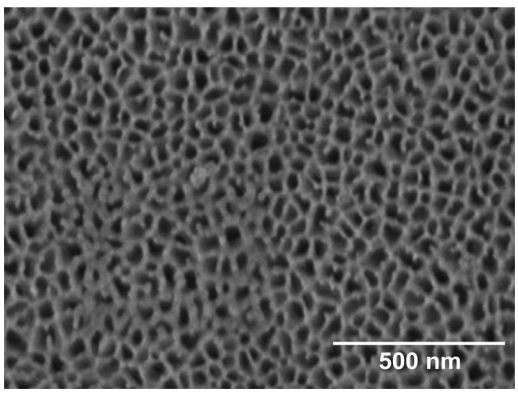

Fig. 1 SEM image of the alumina membrane template, with an averaged porous diameter of about 25 nm.

Characterization

An Hitachi S-3400 scanning electron microscope (SEM) was used to characterize the average pore size of the AAO membranes and to analyse the morphology of the samples processed by melt and solution wetting. Secondary (SEI) and backscattered electron images (BEI) were obtained using an accelerating voltage of 15 kV and a working distance of 10 mm. Au/Pd ultrathin films were deposited on the sample surfaces to minimize charging effects.

X-ray microdiffraction has been performed at the Microfocus beamline (ID13) at the European Synchrotron Radiation Facility (ESRF), using a wavelength of $\lambda = 0.09951$ nm ($E = 12.459$ keV) and a 1 μm diameter beam. Scanning μ-XRD with steps of 1 μm was performed along the cross-section of the sample, from the residual P(VDF-TrFE) film (bulk) to the nanorod array. The 2D-diffraction patterns were recorded in transmission geometry using a FReLoN charge coupled device (CCD) detector (2048 × 2048 pixels of 51.47 × 50.7 μm^2; 16-bit readout). The sample-to-detector distance was calibrated using an Ag-behenate sample as $D = 86.1$ mm.

Atomic Force Microscopy (AFM) was carried out, by means of a Nano-Scope V from Bruker operating in Scanasyst mode, to investigate the morphology of P(VDF-TrFE) copolymers.

Results and discussion

High aspect ratio (length/diameter) one-dimensional (1D) nanoarrays of P(VDF-TrFE) copolymers supported by a residual polymer film have been prepared by melt and solution template wetting. Inorganic materials like AAO templates are considered as high surface energy materials whereas most liquids, including polymer melts and polymer solutions, are of lower surface energies. Thus, the low-energy polymer melts and solutions can wet the high-energy surfaces easily, filling the membrane nanochannels and leading to polymer nanoarray formation.[22] Fig. 1 shows the SEM image of the AAO template with an average pore diameter of ~25 nm.

X-ray microdiffraction (μ-XRD) experiments using synchrotron radiation have been carried out at the ID13 beamline (ESRF). Scanning μ-XRD with a 1 μm diameter beam was accomplished along the cross-section of the samples (Fig. 2a) with diffraction patterns collected at regular intervals between the residual polymer film (bulk) and the nanorod array. The sample's nanorod axis was carefully aligned perpendicular to the X-ray beam, and the 2D-diffraction patterns were recorded in transmission geometry as shown in Fig. 2b.

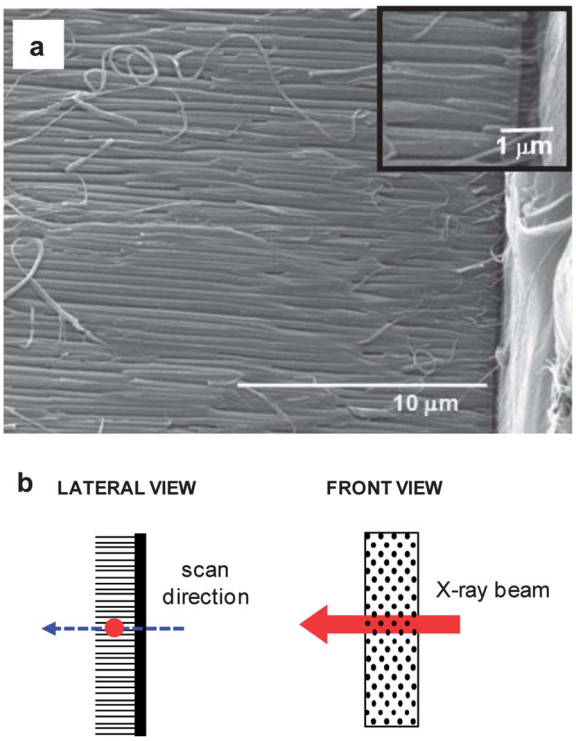

Fig. 2 (a) SEM image of the cross-section of a sample infiltrated by solution wetting and fractured in liquid nitrogen. The inset is a magnified image of the interface between the residual polymer film (right) and the nanorod array into the alumina membrane (left). (b) Schematic diagram of the scanning μ-XRD set-up. The sample was mounted in such a way that the long axes of the PVDF nanorods inside the membrane pores were aligned perpendicular to the synchrotron beam.

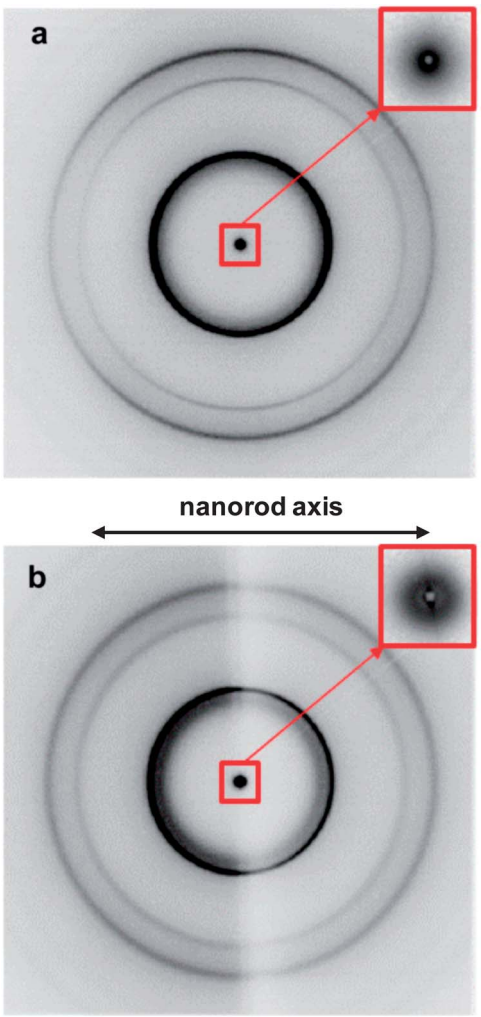

Fig. 3 2D-X-ray diffraction patterns of the residual P(VDF-TrFE) 70/30 films, recorded in transmission geometry: (a) for the sample prepared by melt wetting and (b) solution wetting. Note that the vertical shadow comes from the sample along the beam path. The small angle X-ray scattering (SAXS) region of the patterns has been enlarged and presented as insets.

Fig. 3a shows the diffraction pattern of the residual P(VDF-TrFE) 70/30 film prepared by melt wetting (MW) and Fig. 3b shows that of the P(VDF-TrFE) 70/30 film prepared by solution wetting (SW). The small angle X-ray scattering (SAXS) region of the patterns have been enlarged and presented with the figure as insets. Similar diffraction patterns are obtained for other P(VDF-TrFE) compositions (*i.e.* 80/20) suggesting that the main structural features depend more on the processing method (*i.e.* melt or solution wetting) than on the copolymer composition.

At a first glance, the wide angle X-ray scattering (WAXS) signal from the MW residual P(VDF-TrFE) 70/30 film appears slightly oriented (Fig. 3a) compared to that of the SW samples from the same material (Fig. 3b). The information obtained from the small angle X-ray scattering is complementary to WAXS due to the difference in length scales being probed. It is worth noting that for both samples the SAXS signals are isotropic.

However, the SAXS signal for the SW sample (Fig. 3b) exhibits a well resolved ring, whereas the SAXS intensity for the MW sample (Fig. 3a) is concentrated around the beam stop. Accordingly, a long period of 15 nm can be derived for the SW sample which is related to the nanostructure of semicrystalline polymers consisting of stacked lamellar crystals separated by amorphous layers.[18,23,24] The MW sample exhibits higher correlation lengths related to a larger polymer long period.

Further analysis of the WAXS patterns reveals that the main differences between patterns (a) and (b) of Fig. 3 involve a crystal phase change. Azimuthally integrating the WAXS region of patterns (a) and (b) as well as those corresponding to P(VDF-TrFE) copolymers with different compositions, the corresponding 1-D intensity profiles are obtained and presented in Fig. 4. Bragg reflections have been indexed according to the ferroelectric (FE) orthorhombic form of pseudo-hexagonal nature and the paraelectric (PE) hexagonal crystalline forms respectively.[25,26] Fig. 4a shows 1-D intensity profiles from MW samples of P(VDF-TrFE) 70/30 and 80/20. In both cases only the ferroelectric phase is observed. However, for the SW samples of P(VDF-TrFE) 70/30 and 80/20, 1-D intensity profiles in Fig. 4b indicate the presence of mixed ferroelectric and paraelectric phases.

Regarding WAXS patterns from the infiltrated polymer material within the AAO membranes, only the ferroelectric phase is observed (Fig. 5a) independent of the copolymer composition and of the infiltration method (see Fig. S2†). It is also worth noting the lack of orientation of the patterns of these

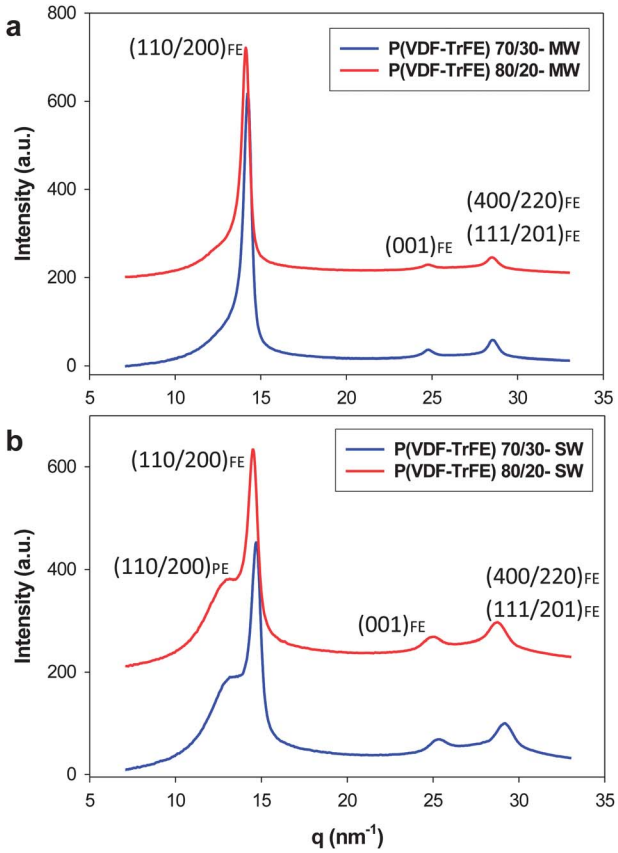

Fig. 4 1-D intensity profiles derived by azimuthal integration of the 2D-diffraction patterns in Fig. 3: (a) for samples prepared by melt wetting (MW) and (b) solution wetting (SW). The *hkl* indices of reflections corresponding to the paraelectric (PE) and ferroelectric (FE) crystalline forms are indicated.

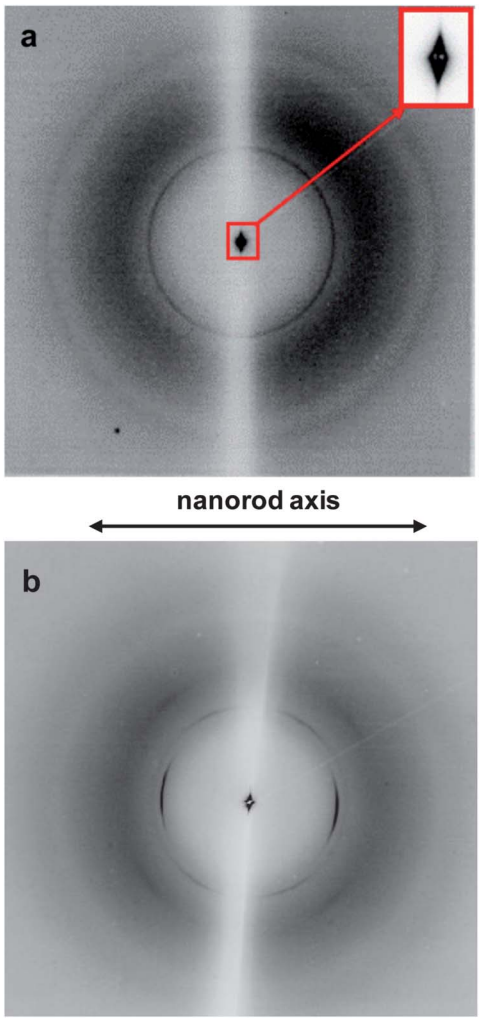

Fig. 5 (a) 2D-diffraction pattern of the P(VDF-TrFE) 80/20 nanorods inside porous alumina prepared by solution wetting. The small angle X-ray scattering (SAXS) region of the pattern has been enlarged and presented in the inset. (b) 2D-diffraction pattern of the homopolymer PVDF nanorods inside porous alumina prepared by solution wetting under the same conditions as (a). Note that the vertical shadow comes also from the sample along the beam path.

ferroelectric copolymers (Fig. 5a) in contrast to the oriented WAXS pattern already reported for the homopolymer PVDF (Fig. 5b).[17] This has also been observed for other polymers infiltrated in AAO membranes.[27] The SAXS pattern of the infiltrated material (inset of Fig. 5a) shows a continuous, oriented scattering on the meridian that mainly corresponds to correlation lengths related to the pores of the AAO membrane and not to the polymer long period. Fig. 6 shows the WAXS intensity profiles (where the contribution from the AAO membrane has been subtracted) for the residual polymer film (upper) and for the polymer nanoarray (bottom) in the case of SW P(VDF-TrFE) 80/20. The deconvolution of the different contributions to the WAXS intensity profiles is also shown by dashed and solid lines. Bragg reflections have been indexed according to the literature.[25,26] Comparing both intensity profiles it can be said that the reflections of the paraelectric phase are absent in the plot for the nanoarray in contrast to the residual polymer film where reflections of both paraelectric and ferroelectric phases are present. This would imply a phase evolution from the mixture of paraelectric and ferroelectric crystal forms (bulk) to a pure ferroelectric one (nanorod array) due to the copolymer confinement within the nanopores of the AAO membrane. This phase change has already been reported for PVDF infiltrated within AAO membranes by solution wetting[17] and for P(VDF-TrFE) 70/30 infiltrated by melt wetting.[7] In the latter case the temperature protocol during melt wetting gave rise to a mixture of both paraelectric and ferroelectric crystal forms for bulk and nanoarrays larger than 40 nm diameter. In the present work, however, we are reporting on the appearance of a pure ferroelectric phase, in both bulk and nanoarrays, for all the P(VDF-TrFE) copolymers infiltrated by melt wetting.

From diffraction patterns collected from the residual polymer film and the nanoarray, several structural features such as crystallinity and crystal phase type can be investigated spatially (Fig. 7). The degree of crystallinity has been calculated from the equation $X_c = \sum I_c / \sum (I_a + I_c)$, where I_c is the integrated area underneath the crystalline peaks and I_a is the integrated area of the amorphous halo, estimated by the peak-fitting of the 1D intensity profiles obtained at each position along the sample cross-section. Fig. 7a shows that the degree of crystallinity is reduced from about 43% in the residual film to about 26% in

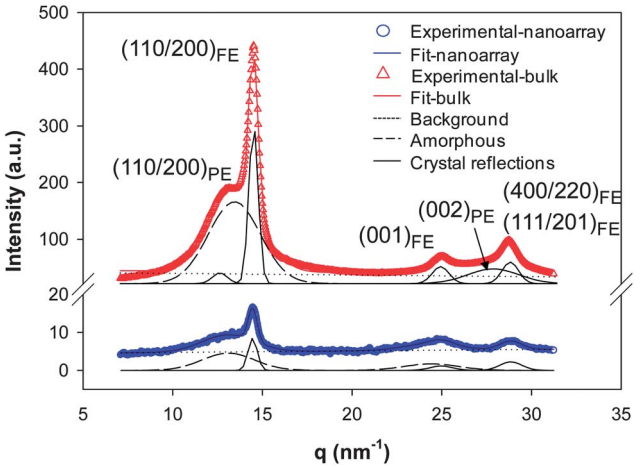

Fig. 6 1D WAXS intensity profiles and their peak-fitting corresponding to the residual polymer film (upper) and to the polymer nanoarray (bottom) for the P(VDF-TrFE) 80/20 prepared by solution wetting. The *hkl* indices of reflections corresponding to the paraelectric (PE) and ferroelectric (FE) crystalline forms are indicated.

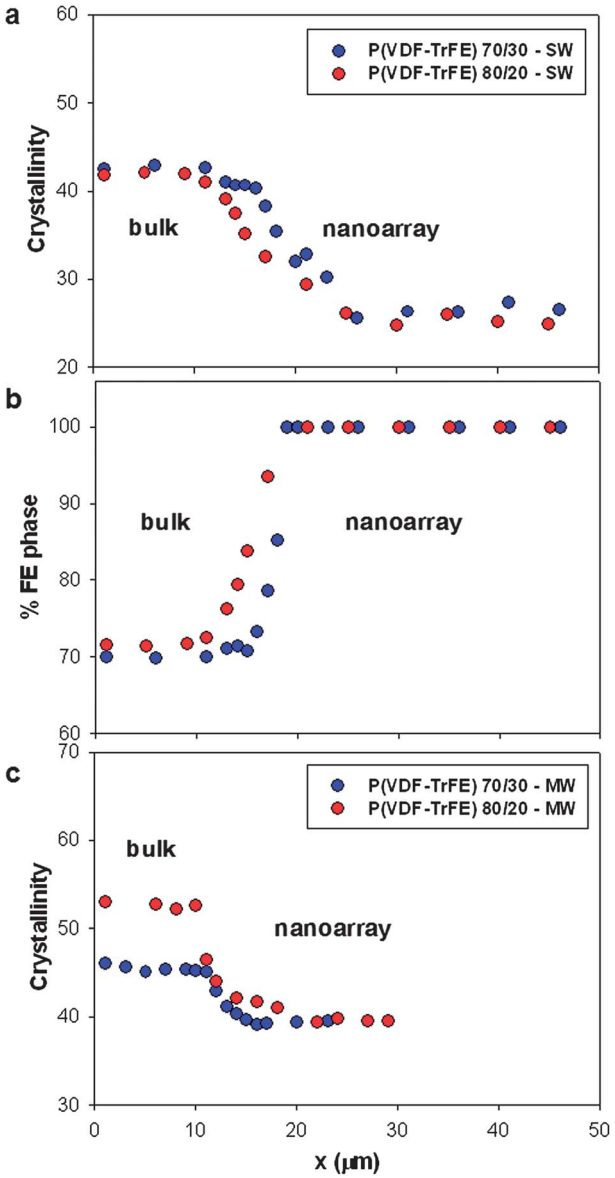

Fig. 7 Spatial evolution, going from the residual polymer film (bulk) towards the nanorod array, of: (a) degree of crystallinity and (b) fraction of the ferroelectric form for samples prepared by solution wetting (SW) and (c) degree of crystallinity for samples prepared by melt wetting (MW).

the nanoarray, for both P(VDF-TrFE) 70/30 and 80/20 prepared by solution wetting. The same behaviour is exhibited by the P(VDF-TrFE) 70/30 and 80/20 samples prepared by melt wetting (Fig. 7c), in this case the degree of crystallinity for the residual film of the 80/20 copolymer (about 53%) is higher than that for the 70/30 copolymer (about 46%) however the crystallinity is reduced to a similar value of about 40% in the nanoarray, a value which is higher than that observed for the SW samples. The partial hindering of crystallization due to a confinement of polymer chains within porous alumina membranes has already been reported.[17,27] The decrease of crystallinity from the residual film to the nanoarray is gradual as it is seen in Fig. 7a and c. The gradient of crystallinity is formed along the first 5–10 microns in the nanorods reaching a steady value afterwards. It is well known that in the bulk polymer crystallization is mainly initiated by heterogeneous nucleation with a relatively small density of nuclei (defects or impurities extrinsic to the polymer), followed by the three-dimensional growth within different morphologies with spherulites dominating.[24] In the particular case of P(VDF-TrFE) random copolymers the characteristic morphology consists of crystalline domains with needlelike shape where each one may be composed of multiple stacks of crystalline lamellae.[23] As shown in Fig. 8a, the morphology of the residual polymer film of SW P(VDF-TrFE) copolymers is characterized by randomly oriented threadlike stacks of crystalline lamellae separated by amorphous layers. Accordingly, a long period of about 17 nm can be derived by AFM (Fig. 8b), which is in agreement with the averaged long period of 15 nm derived by SAXS. This characteristic morphology can explain the lack of orientation in the WAXS patterns of copolymers infiltrated within the AAO membranes (Fig. 5a). For the polymers with spherulitic morphology, which is the case for the homopolymer PVDF, the lamellae in the spherulites are oriented in such a way that the vector of crystallographic plane with the highest growth rate points radially outwards.[28,29] Therefore, lamellae growing along the dominant growth direction are abundant on the surface of the spherulites and grow into the pores they hit, when the spherulites impinge on the surface of the AAO template. Thus a kinetic selection mechanism in the residual film followed by 1D growth along the nanopores, during which the initial orientation is maintained, results in arrays of 1D nanostructures with uniform uniaxial crystal orientation.[15,17,27] However, for the P(VDF-TrFE) copolymers with a morphology characterized by randomly oriented threadlike stacks of crystalline lamellae, statistically growing lamellae in all directions will impinge the surface of the AAO membrane and will grow into the pores they hit. Thus no preferent crystal orientation is found in the nanoarrays.

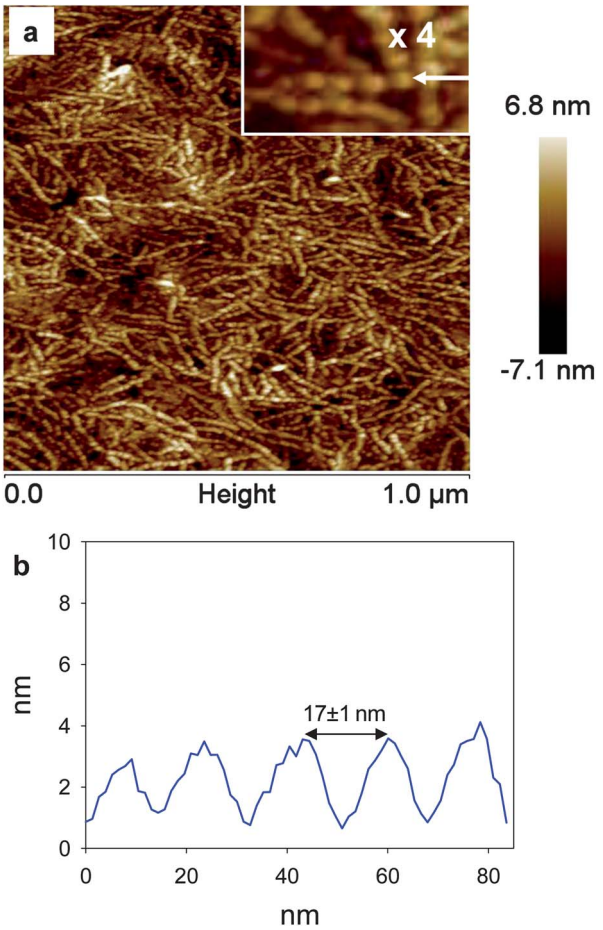

Fig. 8 (a) AFM height image (1 × 1 μm^2) of the residual film of P(VDF-TrFE) 70/30 prepared by solution wetting. The inset shows a magnified image (4×). (b) Height profile obtained along the region pointed by the arrow shown in the inset of (a).

If we assume that the crystallites formed in the bulk can extend within the nanopores only when the nanopore axis is parallel to the growing direction of the lamella, then only some pores will be filled by the crystals growing parallel to the pore axes. In contrast, those crystals reaching the AAO surface not completely parallel to the pore axes will start to grow into the pore but after a short extension the growth will be frustrated by the pore wall. Therefore the nuclei formed in the bulk are expected to induce the crystallization of the polymer at the bottom of the nanorods.[15,27,30]

It is worth mentioning that going away from the residual polymer film into the nanorods, due to their very small volume, the probability of finding heterogeneous nuclei is very low and thus only homogeneous nucleation may appear in those nanorods free of impurities.[14]

The spatial evolution of the two different polymorphs from the PE crystal form (bulk) to the FE form (nanorod array) in the samples prepared by solution wetting is shown in Fig. 7b. The fraction of the ferroelectric phase X_{FE} was estimated from the relationship between the integrated area underneath the PE and FE crystal peaks, $X_{FE} = \sum I_{FE}/\sum(I_{PE} + I_{FE})$. The phase evolution observed can be explained considering that in confined geometries crystallization of the FE phase is preferred because the FE crystal form is denser than the PE form,[18,24] *i.e.* chains are more efficiently packed in the FE phase. This could also explain the lower crystallinity due to confinement achieved for the SW samples compared to the MW ones (Fig. 7a and c). For the MW samples, the residual polymer film already crystallizes in the FE crystal form and these crystallites can extend within the nanorods, whereas for the SW samples the residual polymer film presents a fraction of the PE phase that is inhibited under confinement.

Conclusions

High aspect ratio (length/diameter) one-dimensional (1D) nanoarrays of P(VDF-TrFE) copolymers supported by a residual polymer film have been prepared by melt and solution wetting, using porous anodic aluminum oxide (AAO) as a template. X-ray microdiffraction (μ-XRD) using synchrotron light has revealed the heterogeneous character of the nanoarrays along the nanorods length. The spatial evolution of different polymorphs from the mixture of paraelectric and ferroelectric crystal forms (bulk) to the pure ferroelectric form (nanorod array) due to the copolymer confinement within the nanopores of the AAO membrane is observed for the samples prepared by solution wetting. Samples prepared by melt wetting however exhibit only the ferroelectric phase for both the residual film and nanoarray. The crystal nuclei formed in the residual polymer film connected to the nanoarray play a key role in determining the formation of a gradient crystallinity distribution, where the crystallinity decreases along the first 5–10 microns in the nanorods reaching a steady value afterwards. The minimum decrease in crystallinity is revealed for the P(VDF-TrFE) 70/30 sample prepared by melt wetting. The above crystallization features of P(VDF-TrFE) copolymers under confinement indicate potential for optimizing the ferroelectric character of polymer nanostructures.

Acknowledgements

The authors are grateful for the financial support from the MINECO (grants MAT2011-23455 and FPI BES-2010-030074) and from the CSIC and Fondo Social Europeo (FSE) (JAE-Doc contract), Spain. We thank P. Poza for SEM micrographs and M. Burghamer for his support during measurements at ESRF.

Notes and references

1 R. C. Naber, C. Tanase, P. W. Blom and G. H. Gelink, *Nat. Mater.*, 2005, **4**, 243–248.
2 A. J. Lovinger, *Science*, 1983, **220**, 1115–1121.
3 Y. J. Park, S. J. Kang, C. Park and B. Lotz, *Macromolecules*, 2008, **41**, 109–119.
4 S. J. Kang, I. Bae, Y. J. Shin, Y. J. Park, J. Huh, S. M. Park, H. C. Kim and C. Park, *Nano Lett.*, 2011, **11**, 138–144.
5 Z. Hu, M. Tian, B. Nysten and A. M. Jonas, *Nat. Mater.*, 2009, **8**, 62–67.

6 C.-C. Hong, S.-Y. Huang, J. Shieh and S.-H. Chen, *Macromolecules*, 2012, **45**, 1580–1586.
7 J. L. Lutkenhaus, K. McEnnis, A. Serghei and T. P. Russell, *Macromolecules*, 2010, **43**, 3844–3850.
8 A. Serghei, J. L. Lutkenhaus, D. F. Miranda, K. McEnnis, F. Kremer and T. P. Russell, *Small*, 2010, **6**, 1822–1826.
9 D. R. Rueda, I. Martin-Fabiani, M. Soccio, N. Alayo, F. Pérez-Murano, E. Rebollar, M. C. García-Gutiérrez, M. Castillejo and T. A. Ezquerra, *J. Appl. Crystallogr.*, 2012, **45**, 1038–1045.
10 M. Steinhart, R. B. Wehrspohn, U. Gosele and J. H. Wendorff, *Angew. Chem., Int. Ed.*, 2004, **43**, 1334–1344.
11 J. Martín and C. Mijangos, *Langmuir*, 2009, **25**, 1181–1187.
12 X. Feng and Z. Jin, *Macromolecules*, 2009, **42**, 569–572.
13 J. W. P. Schmelzer and A. S. Avyzov, *J. Chem. Phys.*, 2011, **134**, 054511.
14 H. Duran, M. Steinhart, H. J. Burr and G. Floudas, *Nano Lett.*, 2011, **11**, 1671–1675.
15 M. Steinhart, P. Goring, H. Dernaika, M. Prabhukaran, U. Gosele, E. Hempel and T. Thurn-Albrecht, *Phys. Rev. Lett.*, 2006, **97**, 027801.
16 H. Wang, J. K. Keum, A. Heltner and E. Baer, *Science*, 2009, **323**, 757–760.
17 M.-C. Garcia-Gutierrez, A. Linares, J. J. Hernandez, D. R. Rueda, T. A. Ezquerra, P. Poza and R. J. Davies, *Nano Lett.*, 2010, **10**, 1472–1476.
18 F. J. Baltá Calleja, A. G. Arche, T. A. Ezquerra, C. Santa Cruz, F. Batallán, B. Frick and E. López Cabarcos, *Adv. Polym. Sci.*, 1993, **108**, 1–48.
19 S. J. Kang, Y. J. Park, J. Y. Hwang, H. J. Jeong, J. S. Lee, K. J. Kim, H.-C. Kim, J. Huh and C. Park, *Adv. Mater.*, 2007, **19**, 581–586.
20 E. López Cabarcos, T. A. Ezquerra and F. J. Baltá Calleja, *Macromolecules*, 1998, **31**, 6157–6163.
21 M. K. Lee and J. Lee, *Cryst. Growth Des.*, 2013, **13**, 671–678.
22 P. D. Mingfu Zhang, J. T. Chen and T. P. Russell, *Nano Lett.*, 2006, **6**, 1075–1079.
23 Y. J. Park, S. J. Kang, C. Park and B. Lotz, *Macromolecules*, 2008, **41**, 109–119.
24 G. Strobl, *The Physics of Polymers*, Springer-Verlag, 2007.
25 E. Bellet-Amalric and J. Legrand, *Eur. Phys. J. B*, 1998, **3**, 225–236.
26 R. Su, J. K. Tseng, M. S. Lu, M. Lin, Q. Fu and L. Zhu, *Polymer*, 2012, **53**, 728–739.
27 H. Wu, Z. Su and A. Takahara, *Soft Matter*, 2012, **8**, 3180–3184.
28 A. J. Lovinger and T. T. Wang, *Polymer*, 1979, **20**, 725–731.
29 A. J. Lovinger, *J. Polym. Sci., Polym. Phys. Ed.*, 1980, **18**, 793–799.
30 Z. Hu, G. Baralia, V. Bayot, J.-F. Gohy and A. M. Jonas, *Nano Lett.*, 2005, **5**, 1738–1743.